Supporting Information for

Highly efficient semi-hydrogenation in strained ultrathin PdCu shell and the atomic deciphering for the unlocking of activity-selectivity

Fan Xue[1], Qiang Li[1,*],Weihua Ji[2], Mingxin Lv[1], Hankun Xu[1], Jianrong Zeng[3,4], Tianyi Li[5], Yang Ren[6], Lihui Zhou[7], Xin Chen[1], Jinxia Deng[1], Kun Lin[1], Xianran Xing[1,*]

[1] Beijing Advanced Innovation Center for Materials Genome Engineering, Institute of Solid State Chemistry, University of Science and Technology Beijing, Beijing 100083, China;

[2] College of Materials Science and Engineering, Taiyuan University of Technology, Taiyuan 030024, China;

[3] Shanghai Synchrotron Radiation Facility, Shanghai Advanced Research Institute, Chinese Academy of Sciences, 201204 Shanghai, P. R. China;

[4] Shanghai Institute of Applied Physics, Chinese Academy of Sciences, 201800 Shanghai, P. R. China;

[5] X-Ray Science Division, Argonne National Laboratory, Argonne, Illinois 60439, United States;

[6] Department of Physics, City University of Hong Kong, Kowloon, Hong Kong 999077, China;

[7] Key Laboratory for Advanced Materials and Joint International Research Laboratory of Precision Chemistry and Molecular Engineering, Feringa Nobel Prize Scientist Joint Research Center, School of Chemistry and Molecular Engineering, East China University of Science and Technology, Shanghai 200237, China.

Corresponding author: qiangli@ustb.edu.cn, xing@ustb.edu.cn

Experimental Methods.

Materials. Hydrogen tetrachloroaurate trihydrate ($HAuCl_4$ $3H_2O$, 99.9%) was purchased from Shanghai yuanye Bio-Technology Co., Ltd. Palladium chloride ($PdCl_2$, 99%) and copper acetylacetonate ($Cu(acac)_2$, 99%) were purchased from Sigma-Aldrich. Oleylamine (OAm, 70%) and octadecene (ODE, >90%) were obtained from Aladdin. Anhydrous ethanol, n-hexane (C_6H_{12}, ≥99.5%), and acetone (C_3H_6O, ≥99.3%) were purchased from Sinopharm Chemical Reagent Co., Ltd (Shanghai, China). Vulcan-XC 72R carbon black was obtained from Cabot Corporation, USA. High-purity argon gas (Ar, 99.9%) was produced by Beijing Plexus Gas Company. All chemicals and materials were used as is, without further purification.

Synthesis of Au@PdCu core-shell nanoparticles. 0.05 mmol $HAuCl_4.3H_2O$ and 20 ml of oleylamine were placed in a 50 ml three-necked flask. The mixed solution was subjected to ultrasonic stirring for 15 min, then heated to 130 °C and maintained for 1 h. After natural cooling to room temperature, 0.05 mmol $PdCl_2$ and 0.15 mmol $Cu(acac)_2$ dissolved inside 5 ml of oleylamine were added to the flask together. After stirring for 30 min, it was then heated to 230 °C and held for 1h. The whole process was continuously stirred under argon atmosphere. The colloidal products were collected by centrifugation and washed three times with a mixture of n-hexane, ethanol, and acetone.

Synthesis of PdCu alloy nanoparticles. 0.05 mmol $PdCl_2$, 0.15 mmol $Cu(acac)_2$, 6 ml of oleylamine, and 4 ml of octadecene were placed in a 50 ml three-neck flask. After ultrasonic stirring for 30 min, the mixed solution was heated to 120 °C for 20 min, then heated to 230 °C for 3 h. The whole process was continuously stirred under argon atmosphere. After natural cooling to room temperature, the colloidal products were collected by centrifugation and washed three times with a mixture of n-hexane, ethanol, and acetone.

Synthesis of Au nanoparticles. 0.05 mmol $HAuCl_4.3H_2O$ and 20 ml of oleylamine were placed in a 50 ml three-necked flask. The mixed solution was subjected to ultrasonic stirring for 15 min, then heated to 130 °C and maintained for 1 h. The whole process was continuously stirred under argon atmosphere. After natural cooling to room temperature, the colloidal products were collected by centrifugation and washed three times with a mixture of n-hexane, ethanol, and acetone.

Synthesis of nanocatalysts. The obtained nanoparticles and a certain amount of commercial carbon black (XC-72R) were ultrasonically dispersed in n-hexane for half an hour, respectively, and subsequently placed together in a beaker and stirred for 12 h, so that the nanoparticles were completely loaded on carbon black. The products were then washed with n-hexane and dried at 60 °C overnight. The prepared nanocatalysts were reduced under a $10\%H_2/90\%N_2$ gas stream at 180 °C for 1h and used for the next series of characterizations.

General characterizations. The morphology and size of Au@PdCu, PdCu, and Au nanoparticles were obtained on a HT7700 microscope operated at 100 kV. HRTEM images of Au and PdCu nanoparticles were acquired using a JEM-2010 microscope. The TEM samples were prepared by dropping dilute hexane dispersions of nanocrystals onto a carbon-coated copper grid and then evaporating at room temperature. Aberration-corrected STEM characterization was performed on a ThermoFisher Themis Z microscope equipped with two aberration correctors under 300 kV. The high-angle annular dark-field scanning transmission electron microscopy (HAADF-STEM) images were obtained using a convergence semi-angle of 25 mrad and inner and outer collection angles of 47 and 200 mrad, respectively. Energy-dispersive X-ray spectroscopy (EDS) was carried out using 4 in-column Super-X detectors. The crystal structures of nanoparticles were confirmed by X-ray diffractometer (SmartLab 9 kw, Rigaku Corporation) with Cu Kα radiation. The scanning angle is 20 ~ 90° with 10°/min of scanning speed. X-ray photoelectron spectroscopy (XPS) was acquired on an Axis Supra spectrometer (Kratos, Japan) with Al Kα radiation (1486.6 eV). Au 4f, Pd 3d,

and Cu 2p spectra were analyzed using XPSPEAK software with C 1s at 284.8 eV as calibration. Thermal analysis of coke deposition on used catalysts was performed on a STA 8000 Simultaneous Thermogravimetric analyzer. The actual loadings of Au, Pd, and Cu are obtained by inductively coupled plasma optical emission spectroscopy (Agilent ICPOES 730).

X-ray absorption spectroscopy measurement. In order to obtain the average local coordination structure of Au@PdCu core-shell nanoparticles, Au L_3-edge and Pd K-edge X-ray absorption fine structure (XAFS) spectra were collected on the BL01B1 beamline at SPring-8. Cu K-edge XAFS spectra were collected on the BL13SSW beamline at Shanghai Synchrotron Radiation Facility (SSRF). All samples were pre-reduced at 180 °C under a 10% H_2/N_2 atmosphere for 1 h prior to characterization. The data about the Au L_3-edge (E = 11919 eV), Pd K-edge (E = 24350 eV), and Cu K-edge (E = 8979 eV) were collected at room temperature in transmission mode. The Athena software package processed the raw data, and the EXAFS oscillation function was fitted by Artemis software.[1] Wavelet transform (WT) of Pd K-edge and Au L_3-edge EXAFS oscillations was implemented using the HAMA software module developed by Harald and Marina Chukalina.

Total scattering measurement. The high energy X-ray scattering data was collected on the 11-ID-C beamline at the Advanced Photon Source (APS) of Argonne National Laboratory with the X-ray wavelength of 0.1173 Å. The atomic pair distribution function (PDF) was obtained by direct Fourier transform of reduced structure function with a Q value of 24 $Å^{-1}$ by PDFgetX2 software.[2] The unit cell parameters of the core and shell portions of the Au@PdCu nanoparticles were obtained by small box fitting based on PDFgui.[3] Based on the framework of FCC unit cells of Au@PdCu nanoparticles derived through small box fitting, structural models matching to the size of core and shell Au@PdCu nanoparticles were established by random substitution of Au, Pd or Cu in terms of trimetallic chemical components containing about 83486 atoms, respectively, and then placed into the middle of a 200Å*200Å*200Å vacuum

box as the initial model of RMC. A big box fitting for PDF data was carried out by RMCprofile.[4] DISCUS software was utilized to analyze the local coordination environment and atomic spatial distribution.[5]

Catalytic performance measurement. Selective hydrogenation of acetylene in excess ethylene was carried out in a fixed-bed microreactor at ambient pressure with a space velocity (GHSV) of 112500 $mLh^{-1}g^{-1}$. The reaction gases consisted of 0.33 % C_2H_2, 32.98% C_2H_4, and 0.66% H_2, with N_2 as the balance gas. The whole flow rate was maintained at 75 ml/min. Specifically, approximately 40 mg of catalyst samples were first mixed with 1460 mg of quartz sand and pretreated under a 10%H_2/N_2 atmosphere at 180 °C for 1 h. After cooling to room temperature in N_2, the catalytic evaluation was performed at 30-180 °C. It was required to hold each temperature point for 30 min in order to establish a more stable state and then to conduct multiple tests to guarantee reproducibility. The outlet gases were analyzed by online gas chromatography (GC) with a flame ionization detector using a PLOT capillary column (50 mm × 0.53 mm). The acetylene conversion, ethylene selectivity, GHSV, and specific activity were calculated using equations, respectively.

$$\text{Acetylene conversion (\%)} = \frac{C_2H_2(\text{inlet}) - C_2H_2(\text{outlet})}{C_2H_2(\text{inlet})}$$

$$\text{Ethene selectivity (\%)} = \frac{C_2H_4(\text{outlet}) - C_2H_4(\text{inlet})}{C_2H_2(\text{inlet}) - C_2H_2(\text{outlet})}$$

$$\text{GHSV(mL.g - 1.h - 1)} = \frac{F}{mcat}$$

$$\text{Specific activity} = \frac{\text{GHSV} \times C_2H_2(\text{inlet}) \times \text{C2H2 conversion} \times \text{MPd}}{\text{wPd} \times 22.4 \times 103}$$

Here, C_2H_2 (inlet) and C_2H_2 (outlet) are the acetylene concentrations at the inlet and outlet of the reactor, respectively. C_2H_4 (inlet) and C_2H_4 (outlet) are the ethene concentrations at the inlet and outlet of the reactor, respectively. F is the total gas flow, and m_{cat} is the catalyst mass. M_{Pd} is the relative atomic mass of the active metal Pd, and w_{Pd} is the loading of the active metal Pd.

The dispersion (D) of active metal was estimated using the hemisphere model in order to calculate the turnover frequency (TOF).

$$D = \frac{Sparticle / Satom}{Vparticle / Vatom} = \frac{4 \times datom}{dparticle}$$

$$TOF = \frac{Specific\ activity}{D}$$

The values of $S_{particle}$ and S_{atom} correspond to the surface area of a metal particle and the cross-section area of a metal atom, respectively; $V_{particle}$ and V_{atom} represent the volume of a metal particle and volume of a metal atom, while $d_{particle}$ and d_{atom} represent the average size of a metal particle and the diameter of a metal atom. The apparent activation energies were determined using a reaction temperature where acetylene conversion was below 20%.

Density Functional Theory (DFT) Calculations. All the DFT calculations were carried out with the projector augmented wave (PAW) using the Vienna ab initio simulation package (VASP)[6,7]. Adopting the exchange–correlation functional of Perdew–Burke–Ernzerh[8] within the generalized gradient approximation (GGA)[9,10], the cut-off energy for the basis set was chosen as 400 eV. Brillouin zone was sampled by a 4×4×1 k-mesh. The energy difference of 1.0×10^{-5} eV per atom and the max force of 0.01 eV/Å were set as the convergence criteria for geometry optimization and subsequent analysis. The projected density of states (PDOS) is calculated based on the geometrically optimized models. The origin models were constructed on the PdCu (111) surface with 4-layer atoms, where the Pd and Cu atomic ratios are consistent with the ICP results. The structure models with 0%, 1.6%, and 3.25% lattice strains were created by modifying the parameters of the unit cells, using the average Pd-Pd bond length of the PdCu nanocatalysts obtained by EXAFS as a benchmark. In order to ensure that the active sites on the outermost surface have a similar coordination number, the surface Pd and Cu atoms undergo some substitution. A vacuum layer of 15 Å was set between the periodically repeated slabs to avoid inter-slab interactions.

To understand the excellent catalytic performance of the Au@PdCu catalyst, DFT

calculations were performed on the adsorption energies of hydrogen and ethylene. We constructed the Pd (111) surface model, the 0%-PdCu (111) surface model corresponding to the PdCu nanocatalyst, and the 3.25%-PdCu (111) surface model corresponding to the Au@PdCu nanocatalyst. The ethylene and hydrogen formation adsorption energies were calculated using the following equation:

$$E_{ads} = E_{ad} - E_{sub} - E_{ee}$$

Where E_{ad} is the total energy of the substrate with adsorbed ethylene molecules or hydrogen atom, E_{sub} is the energy of the substrate, and E_{ee} is the energy of the ethylene molecules or hydrogen in the gas phase.

Supplementary Figures and Tables.

Table S1. Chemical compositions and elemental loading amounts of PdCu/C and Au@PdCu/C samples determined by ICP-OES.

Samples	Molar ratios of Au:Pd:Cu	Loading amounts of Pd(wt.%)	Loading amounts of Cu(wt.%)	Loading amounts of Au(wt.%)
PdCu/C	0:38:62	1.15	1.12	—
Au@PdCu/C	28:27:45	0.84	0.83	1.62

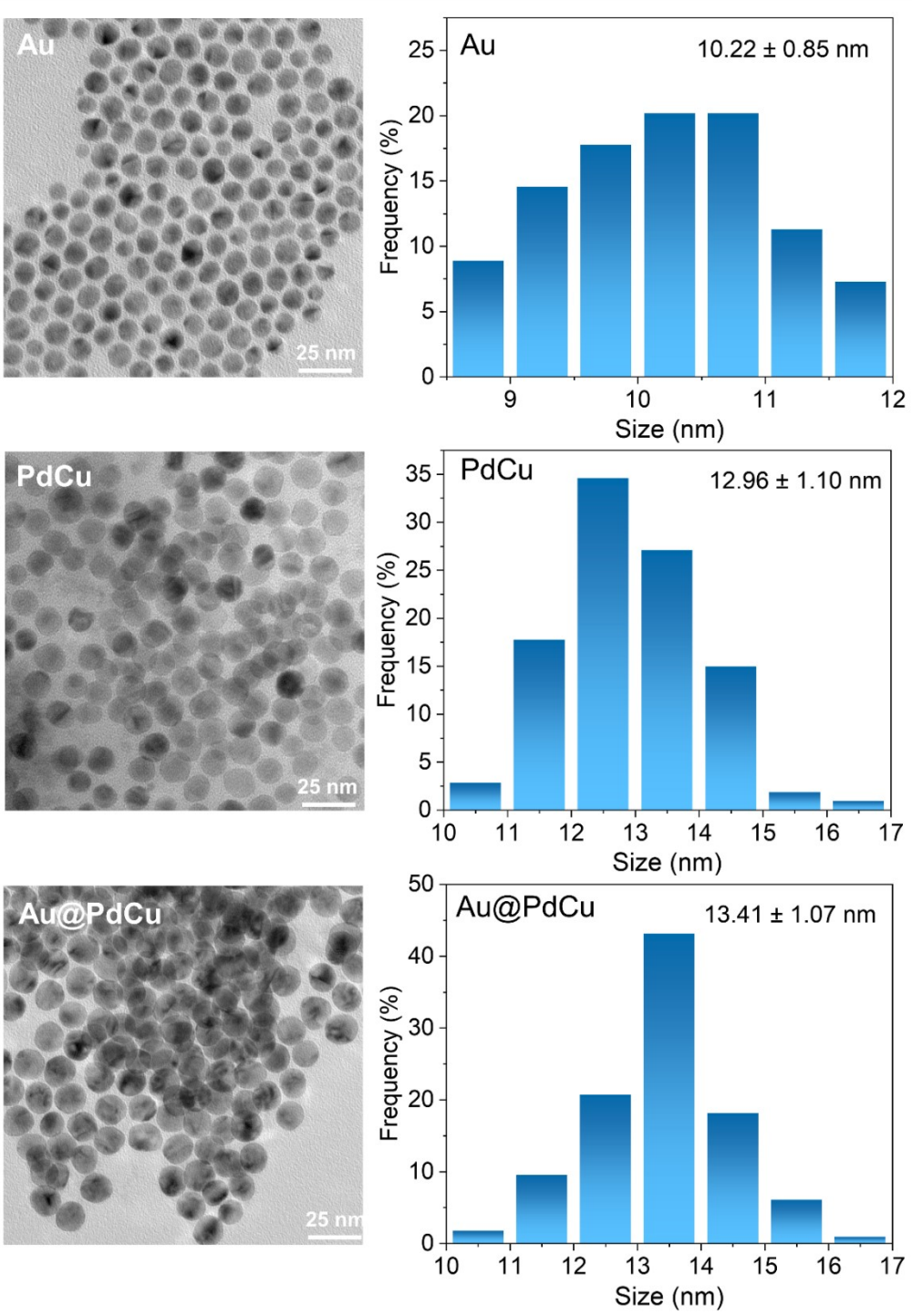

Figure S1. TEM images and size distribution of Au, PdCu, and Au@PdCu NPs

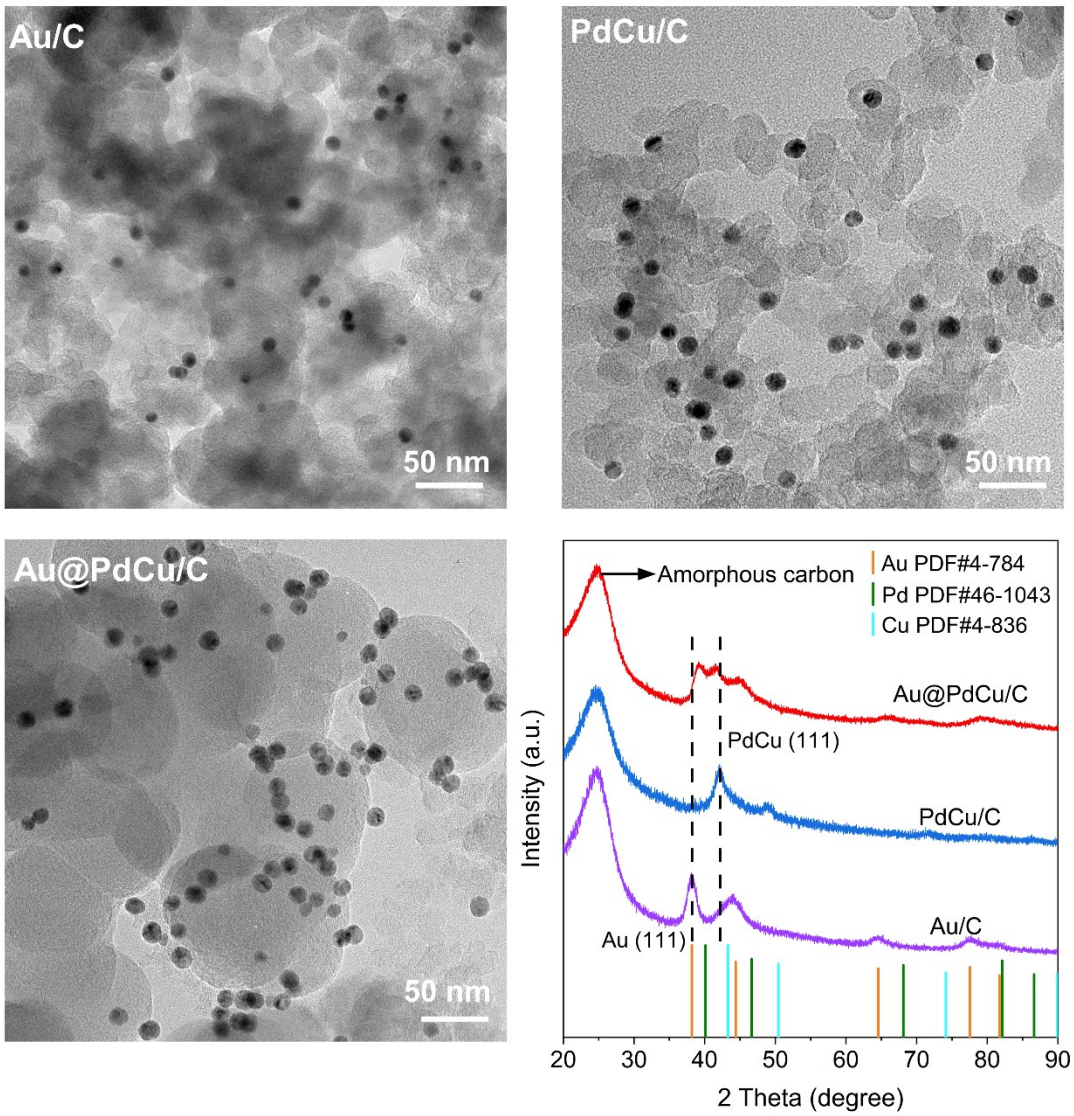

Figure S2. TEM images and XRD patterns of Au/C, PdCu/C, and Au@PdCu/C.

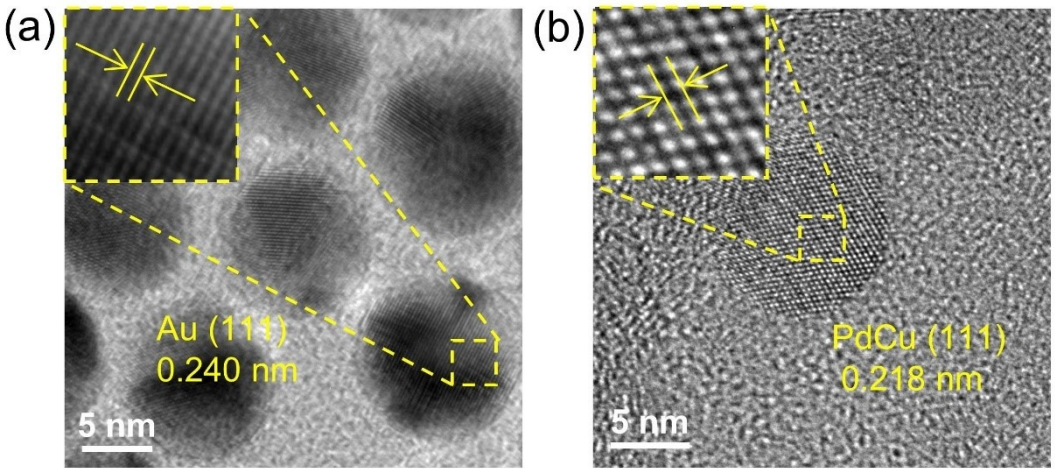

Figure S3. HRTEM images of Au NPs (a) and PdCu NPs (b).

Table S2. Catalytic performances of different catalysts reported in the literature for semi-hydrogenation of acetylene.

Catalysts	Temperature (°C)	Conversion (%)	Selectivity (%)	Reactant (C_2H_2:H_2:C_2H_4)	Ref.
Au@PdCu/C	**122**	**100**	**92.4**	**1/2/99**	**This work**
Pd_2Sn/C	160	97.5	91	1/2/99	11
Pd_1/UIO-66-NH_2	200	100	90	1/2/99	12
Pd_1/ND@G	180	100	90	1/10/20	13
Pd/PPS	100	99	73	1/1.5/82	14
$Ni_3ZnC_{0.7}$/oCNT	200	99	94	1/9/40	15
NiCuFeGaGe/SiO_2	220	100	93	1/10/10	16
Pd-ISAS/CN	100	92	80	0.65/5/50	17
Cu/B2 CuPd-2	80	94.2	87.8	1/10/20	18
$Al_{14}Fe_3$	200	85	84	1/10/100	19
Pd@C/CNT	150	93	70	0.5/3/20	20
Pd_1Cu_1/ND@G	110	100	92	1/10/20	21
Pd_1-Fe/Fe_2O_3	120	100	94.7	1/20/10	22
NiSb	260	100	93.2	1/5/60	23
Pd_2Ga/CNT	200	90	58.1	0.5/5/50	24
Ni_1Cu_2/g-C_3N_4	160	100	90	1/10/50	25
PdZn-1.2@ZIF-8C	120	85	80	0.65/5/50	26
$Cu_{2.75}Ni_{0.25}Fe$	250	100	75	1.5/4.5/8.1	27
$AgPd_{0.01}$/SiO_2	160	93	80	1/20/20	28
ISA-Pd/MPNC	110	100	82	0.5/5/50	29
PdAg NPs/HT	90	90	79	0.35/0.6/32.8	30

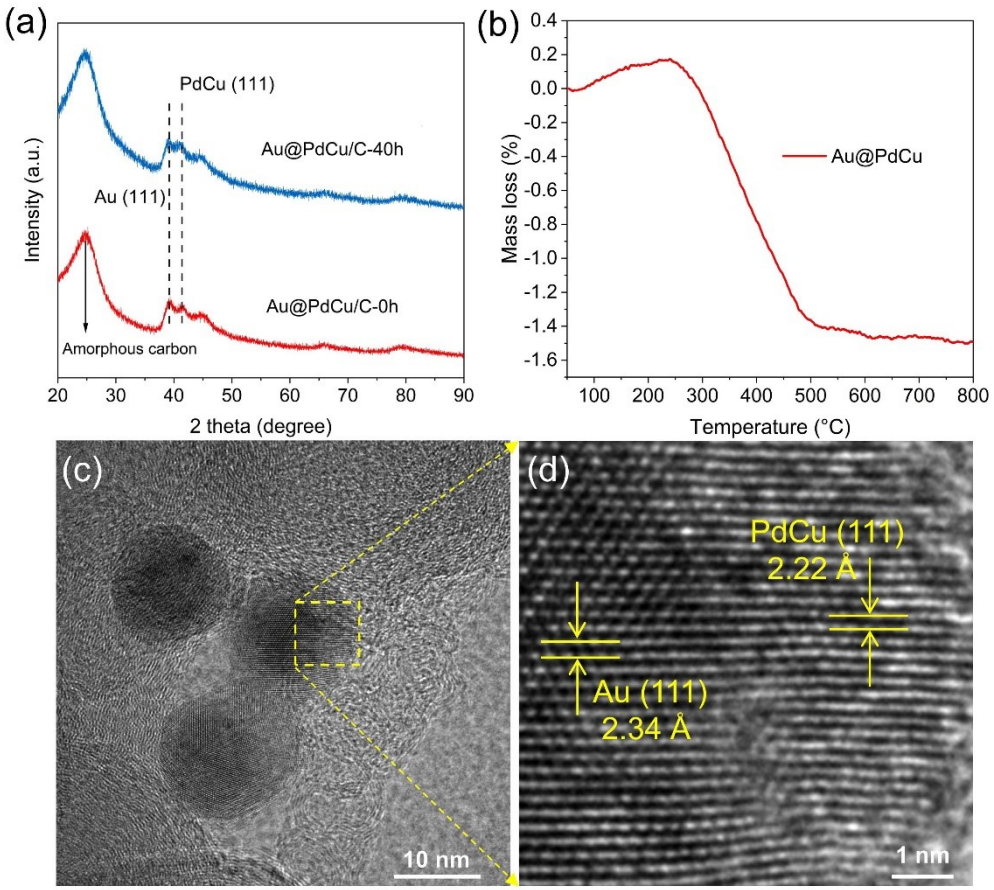

Figure S4. (a) XRD patterns of Au@PdCu/C-0h and Au@PdCu/C-40h. (b) TG curve of Au@PdCu/C-40h. (c) HRTEM image of Au@PdCu/C-40h. (d) Enlarged HRTEM image. Au@PdCu/C-0h is the fresh catalyst. Au@PdCu/C-40h is the catalyst after the 40-hour useage.

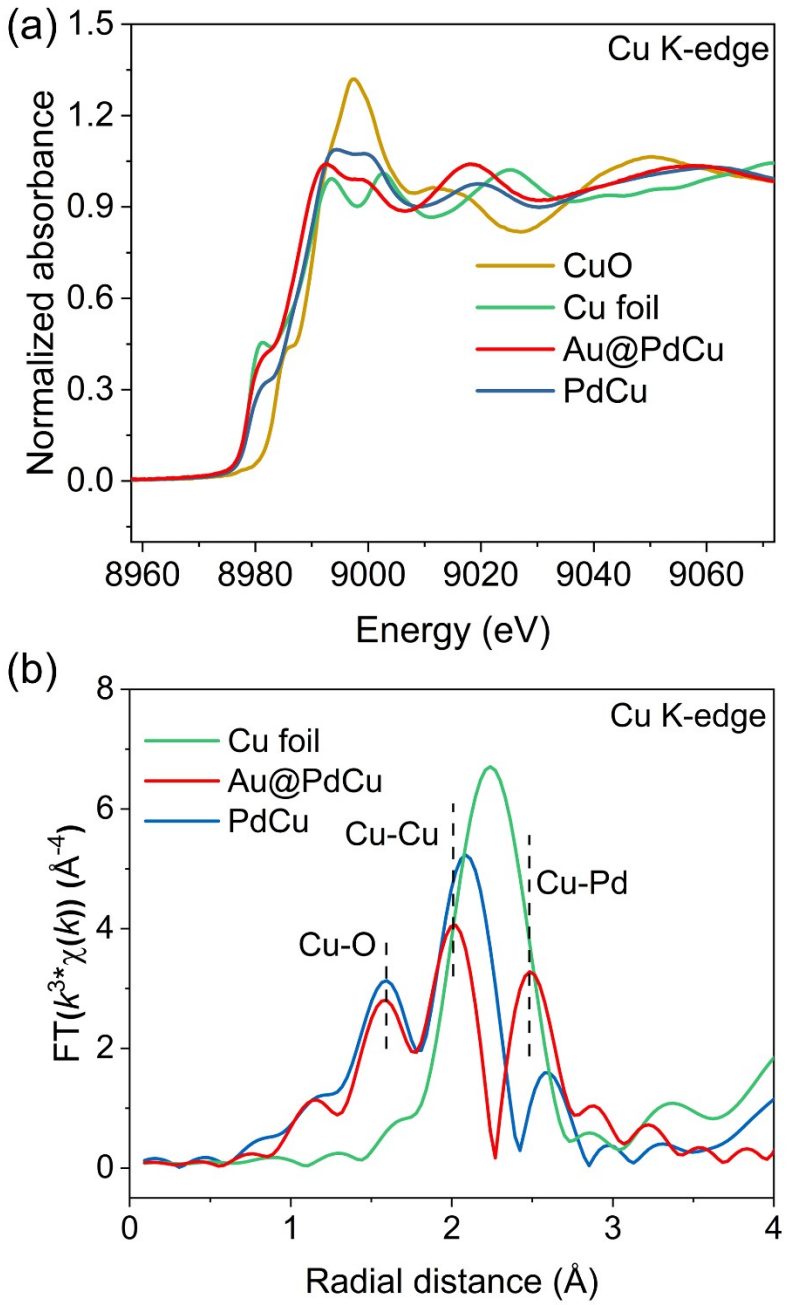

Figure S5. (a) Normalized Cu K-edge XANES spectra of PdCu, Au@PdCu, Cu foil, and CuO. (b) k^3-weighted Fourier transform Cu K-edge EXAFS spectra.

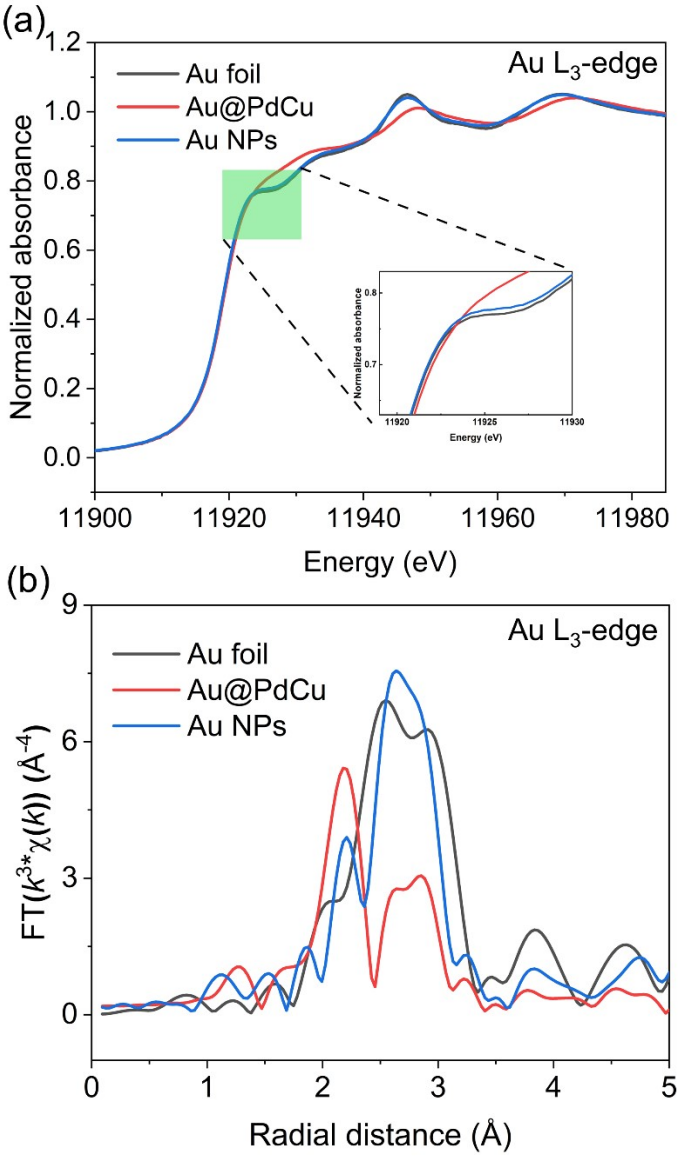

Figure S6. (a) Normalized Au L_3-edge XANES spectra of Au NPs, Au@PdCu, Au foil (b) k^3-weighted Fourier transform Au L_3-edge EXAFS spectra.

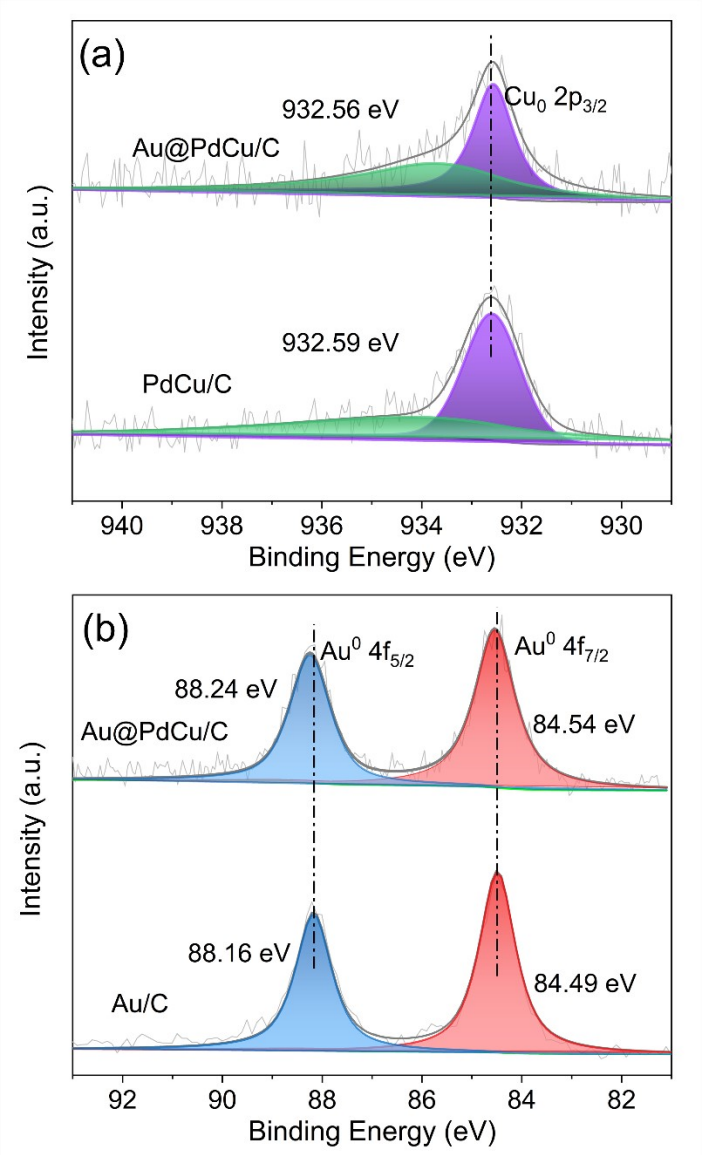

Figure S7. (a) Cu 2p XPS spectra of PdCu/C and Au@PdCu/C catalysts. (b) Au 4f XPS spectra of Au/C and Au@PdCu/C catalysts.

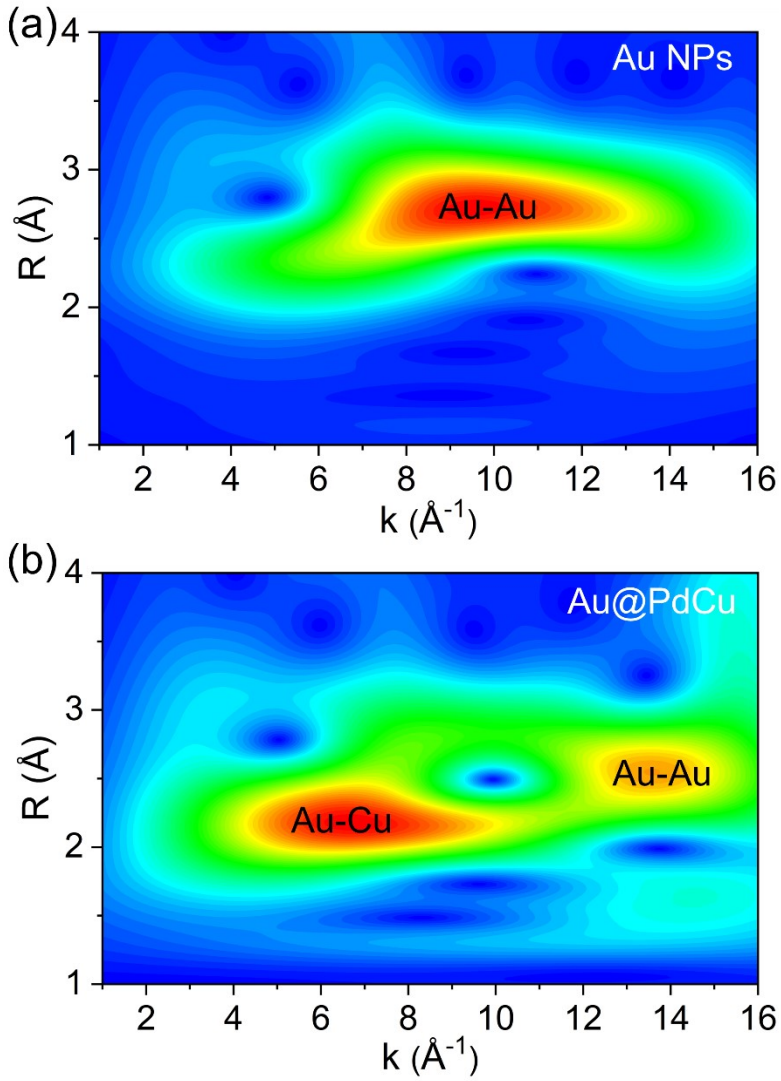

Figure S8. Au L_3-edge WT-EXAFS contours of Au NPs and Au@PdCu catalysts.

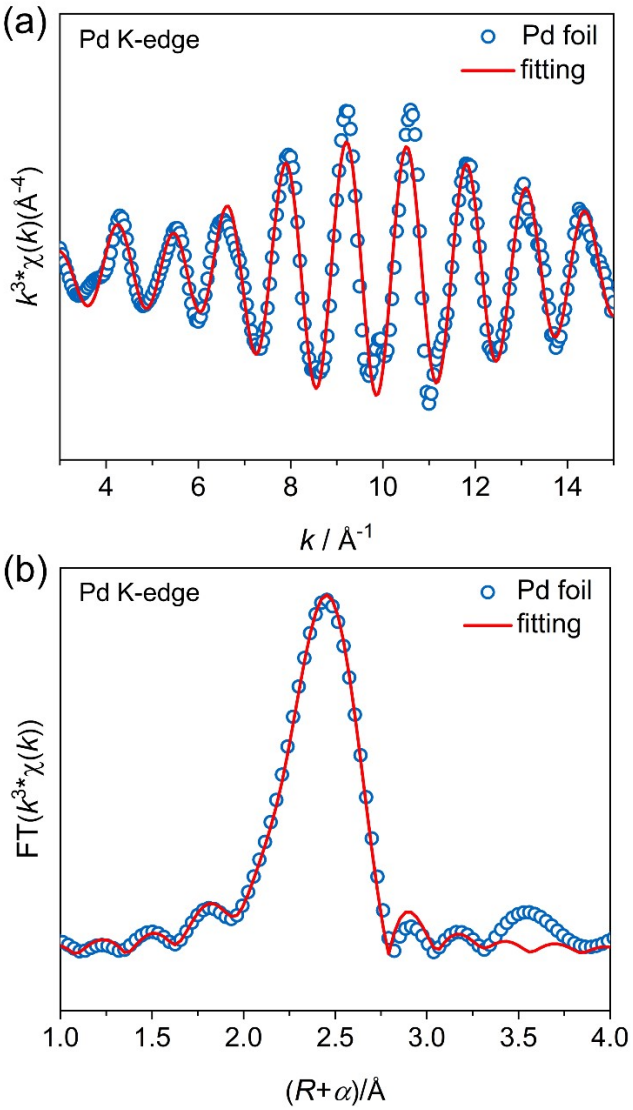

Figure S9. Fitting results of the EXAFS spectra Pd K-edge for Pd foil. (FT range: 3.16 Å^{-1}–14.8 Å^{-1}, Fitting range: 1.00 Å–3.00 Å)

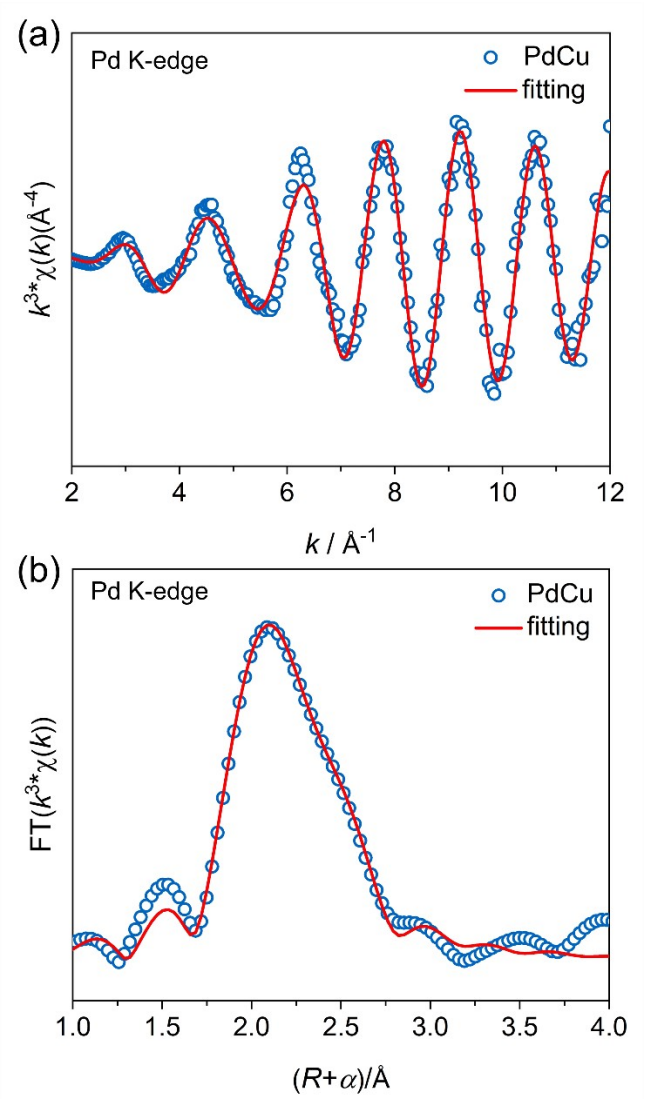

Figure S10. Fitting results of the EXAFS spectra of Pd K-edge for PdCu. (FT range: 2.59 Å^{-1}–11.73 Å^{-1}, Fitting range: 1.0 Å–3.0 Å)

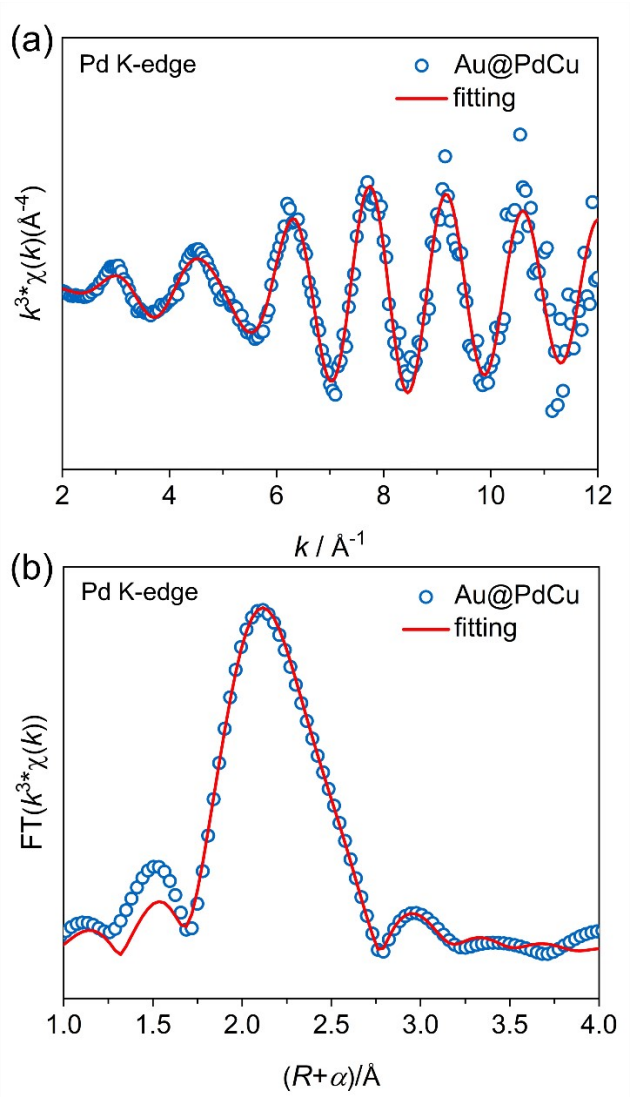

Figure S11. Fitting results of the EXAFS spectra of Pd K-edge for Au@PdCu. (FT range: 3 Å^{-1}–11.87 Å^{-1}, Fitting range: 1.0 Å–3.3 Å)

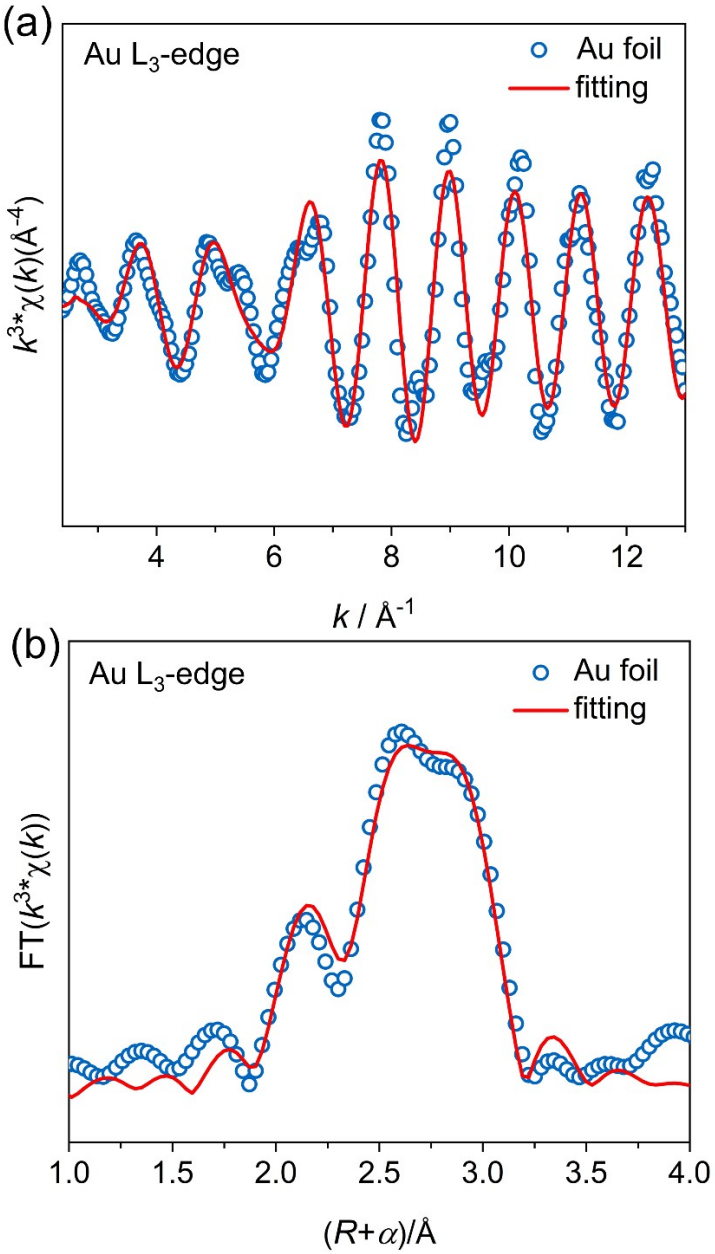

Figure S12. Fitting results of the EXAFS spectra of Au L_3-edge for Au foil. (FT range: 2.48 $Å^{-1}$–13.5 $Å^{-1}$, Fitting range: 1.2 Å–3.2 Å)

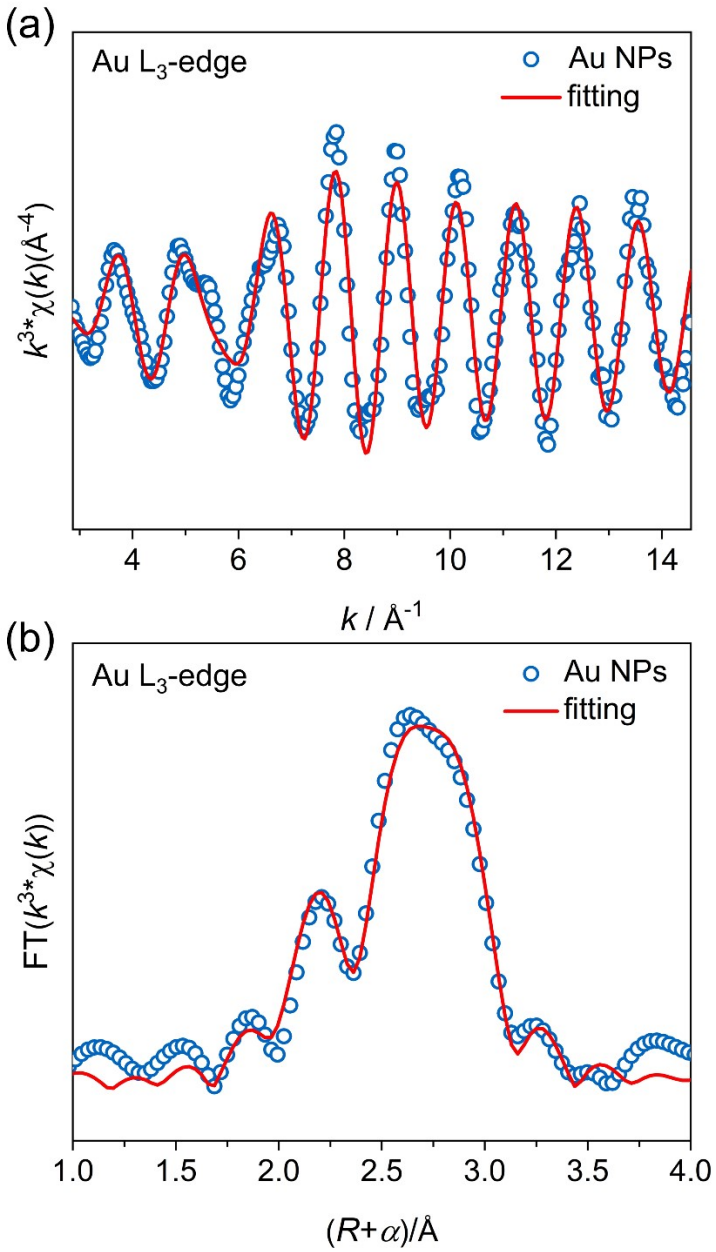

Figure S13. Fitting results of the EXAFS spectra of Au L_3-edge for Au NPs. (FT range: 2.87 $Å^{-1}$–14.55 $Å^{-1}$, Fitting range: 1.25 Å–3.20 Å)

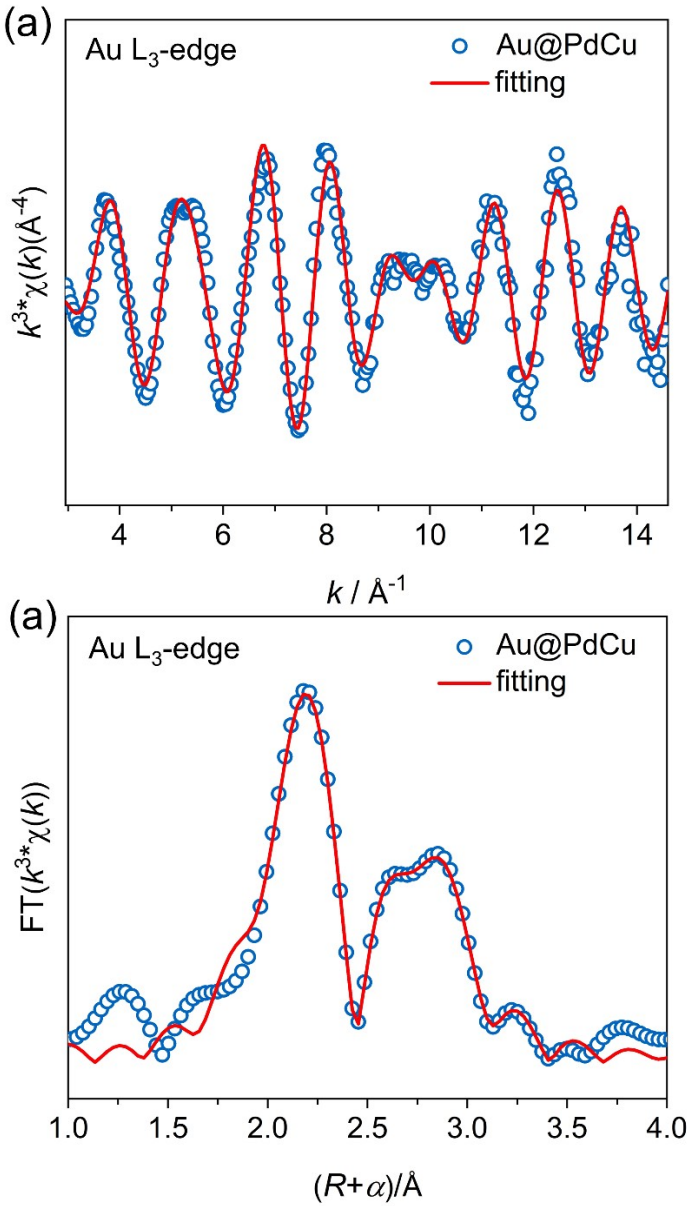

Figure S14. Fitting results of the EXAFS spectra of Au L_3-edge for Au@PdCu. (FT range: 2.95 $Å^{-1}$–14.60 $Å^{-1}$, Fitting range: 1.27 Å–3.20 Å)

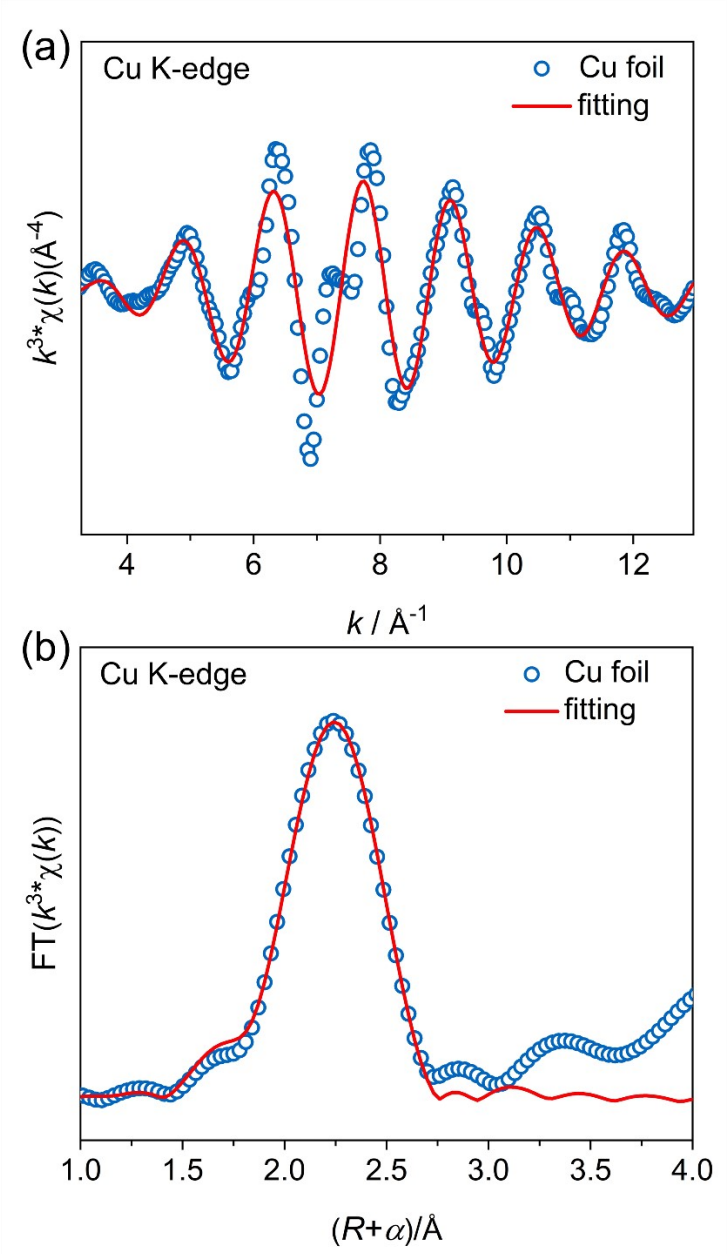

Figure S15. Fitting results of the EXAFS spectra of Cu K-edge for Cu foil. (FT range: 3.28 Å^{-1}–12.95 Å^{-1}, Fitting range: 1.0 Å–3.0 Å)

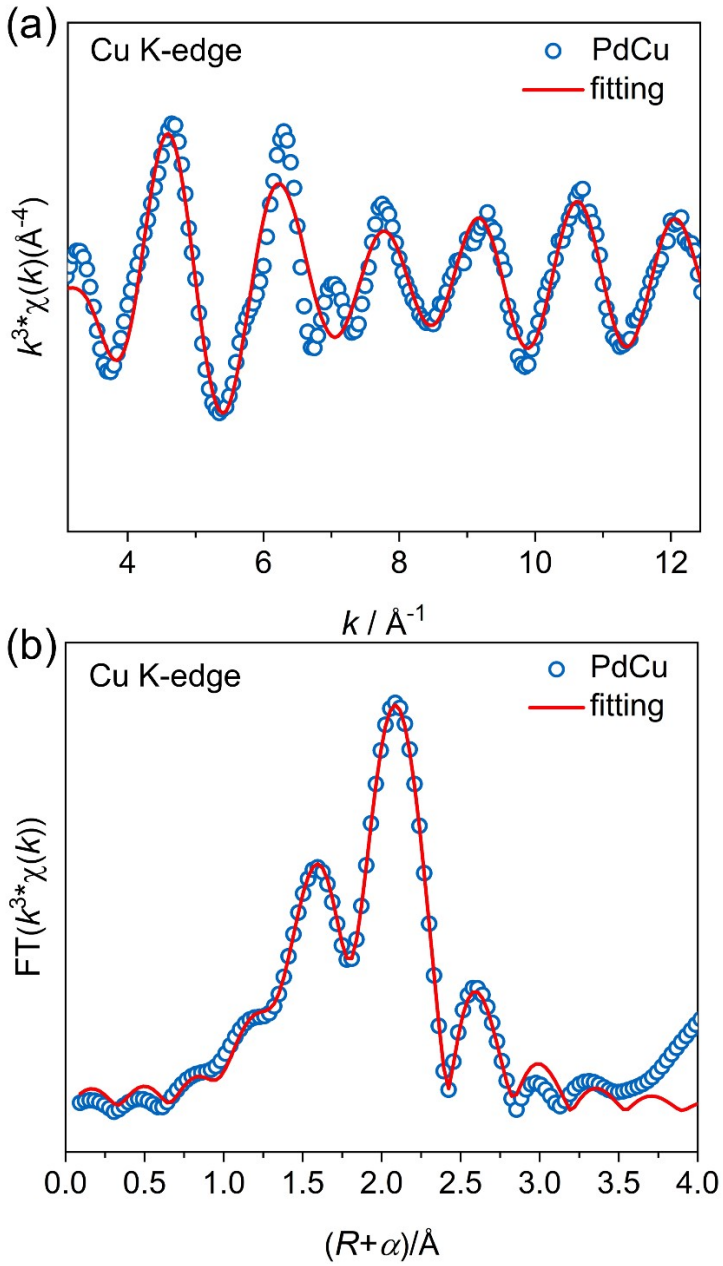

Figure S16. Fitting results of the EXAFS spectra of Cu K-edge for PdCu. (FT range: 3.12 Å^{-1}–12.43 Å^{-1}, Fitting range: 1.0 Å–3.0 Å)

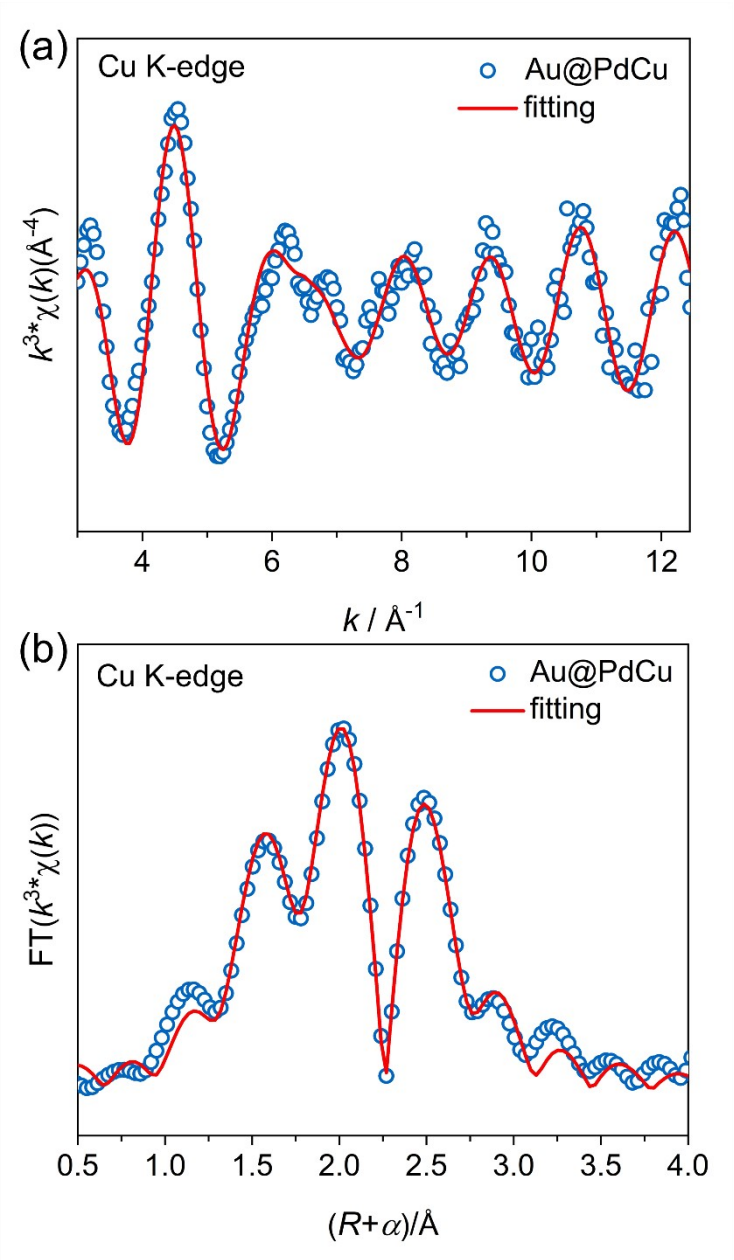

Figure S17. Fitting results of the EXAFS spectra of Cu K-edge for Au@PdCu. (FT range: 3.0 Å^{-1}–12.44 Å^{-1}, Fitting range: 1.1 Å–3.40 Å)

Table S3. Fitting Results of Cu K-Edge EXAFS Data.

Sample	Scattering pair	CN	R (Å)	σ^2 (10^{-3} Å^2)	ΔE_0 (eV)	R factor
PdCu	Cu-O	1.3 ± 0.3	1.946 ± 0.018	7.4 ± 2.5	7.30 ± 2.55	0.002
	Cu-Cu	2.5 ± 0.4	2.562 ± 0.009	6.0 ± 1.4	2.29 ± 1.29	
	Cu-Pd	2.0 ± 0.3	2.583 ± 0.010	6.0 ± 1.4	2.29 ± 1.29	
Au@PdCu	Cu-O	0.8 ± 0.5	1.945 ± 0.045	4.3 ± 5.1	7.16 ± 6.36	0.008
	Cu-Cu	2.0 ± 1.1	2.572 ± 0.033	6.7 ± 5.2	-0.78 ± 2.50	
	Cu-Pd	2.9 ± 1.4	2.583 ± 0.023	6.7 ± 5.2	-0.78 ± 2.50	
	Cu-Au	0.5 ± 0.5	2.621 ± 0.103	5.1 ± 9.4	-0.78 ± 2.50	
Cu foil	Cu-Cu	12	2.541 ± 0.004	8.3 ± 0.5	5.68 ± 0.80	0.005

Table S4. Fitting Results of Pd K-Edge EXAFS Data.

Sample	Scattering pair	CN	R (Å)	σ^2 (10^{-3} Å^2)	ΔE_0 (eV)	R factor
PdCu	Pd-Cu	5.3 ± 0.4	2.594 ± 0.009	7.5 ± 0.7	-9.25 ± 1.51	0.007
	Pd-Pd	3.2 ± 0.4	2.680 ± 0.007	7.5 ± 0.7	-9.25 ± 1.51	
Au@PdCu	Pd-Cu	4.3 ± 0.8	2.601 ± 0.007	7.6 ± 1.4	-7.66 ± 1.32	0.01
	Pd-Pd	2.4 ± 0.5	2.710 ± 0.017	7.6 ± 1.4	-7.66 ± 1.32	
	Pd-Au	2.0 ± 0.7	2.776 ± 0.038	7.6 ± 1.4	-7.66 ± 1.32	
Pd foil	Pd-Pd	12	2.743 ± 0.002	5.8 ± 0.2	-6.31 ± 0.47	0.003

Table S5. Fitting Results of Au L_3-Edge EXAFS Data.

Sample	Scattering pair	CN	R (Å)	σ^2 (10^{-3} Å^2)	ΔE_0 (eV)	R factor
Au@PdCu	Au-Cu	2.5 ± 0.4	2.652 ± 0.012	8.9 ± 0.7	1.74 ± 1.23	0.018
	Au-Pd	1.9 ± 0.5	2.710 ± 0.017	8.9 ± 0.7	1.74 ± 1.23	
	Au-Au	5.4 ± 1.1	2.812 ± 0.006	8.9 ± 0.7	1.74 ± 1.23	
Au NPs	Au-Au	9.6 ± 0.6	2.847 ± 0.003	8.0 ± 0.3	2.22 ± 0.70	0.008
Au foil	Au-Au	12	2.852 ± 0.005	8.1 ± 0.6	2.49 ± 1.25	0.02

The value of S_0^2 is obtained from the fitting for Pd foil, Cu foil, and Au foil (Pd 0.887; Cu 0.75; Au 0.839). CN is the coordination number. R is interatomic distance (the bond length between central atoms and surrounding coordination atoms). σ^2 is Debye-Waller factor (a measure of thermal and static disorder in absorber-scatterer distances). ΔE_0 is edge-energy shift. R factor was applied to evaluate the goodness of the fitting.

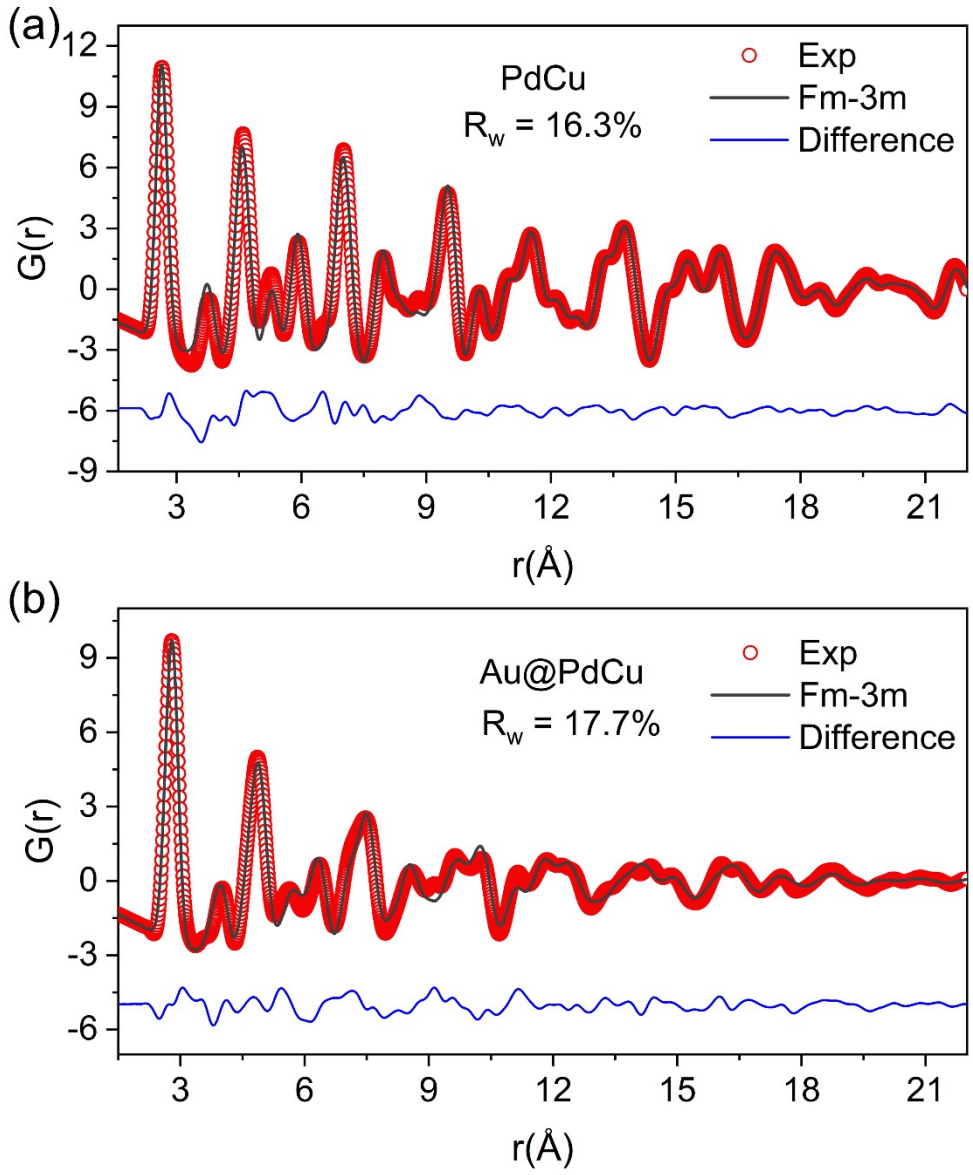

Figure S18. Atomic pair distribution functions and small-box fitting results of PdCu alloy (a) and Au@PdCu core-shell (b) nanoparticles with FCC structure.

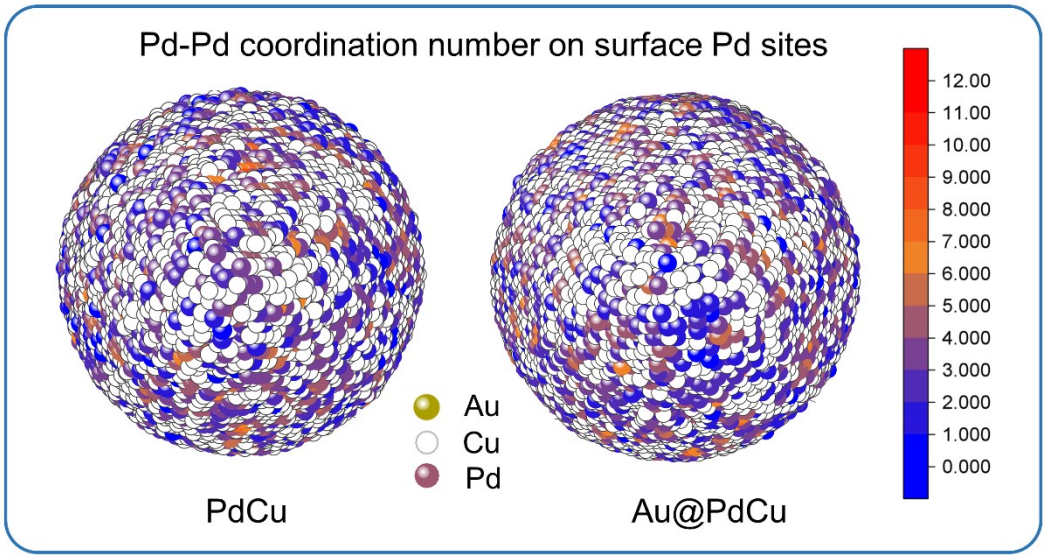

Figure S19. The 3D distribution of the nearest Pd-Pd coordination number on the Pd sites of PdCu and Au@PdCu NPs.

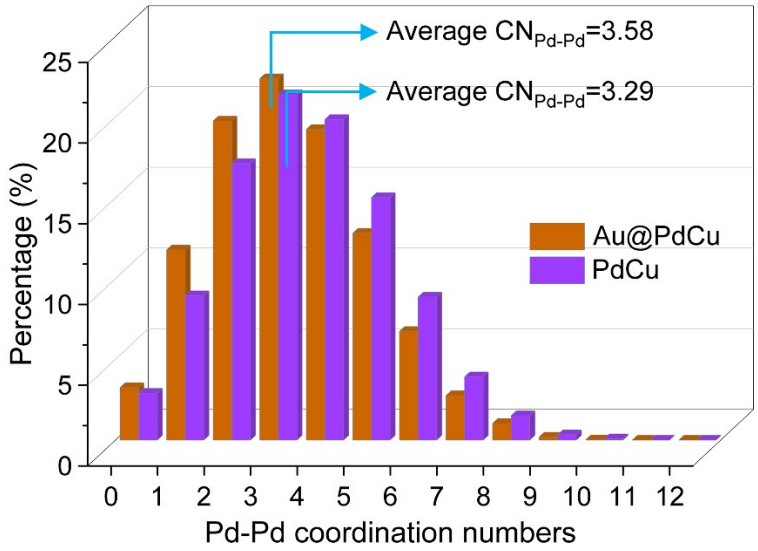

Figure S20. The comparison of surface Pd-Pd coordination number of PdCu and Au@PdCu NPs.

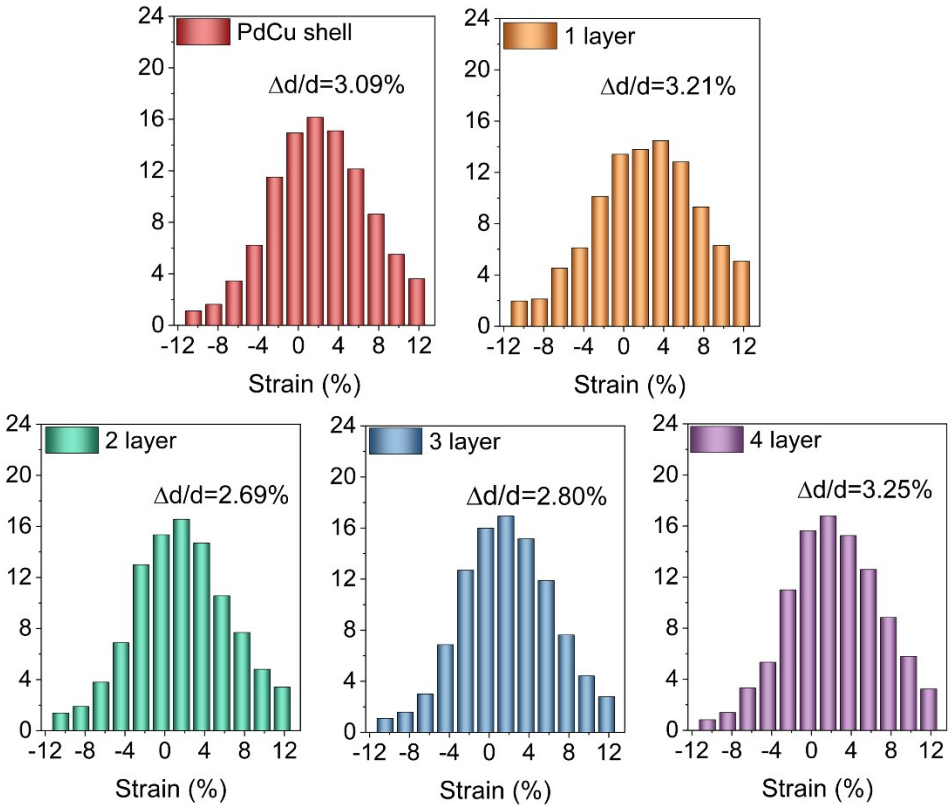

Figure S21. Statistics of surface strain on Pd sites within each layer of the PdCu shell for Au@PdCu NPs.

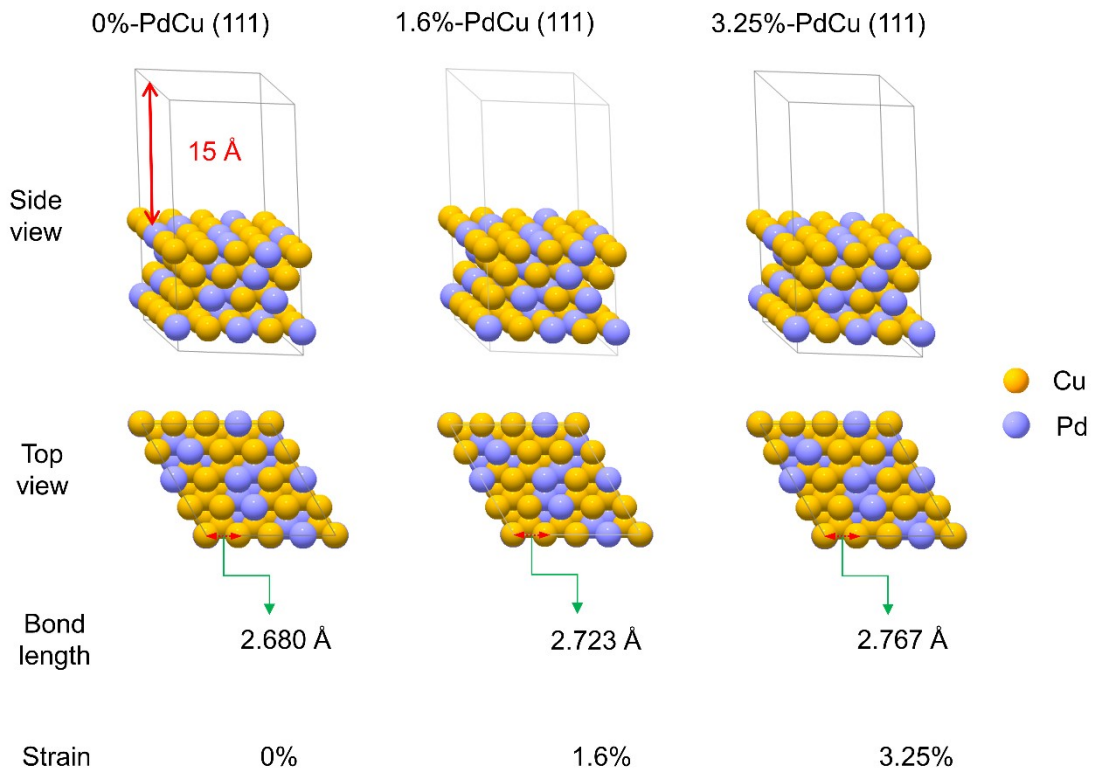

Figure S22. The constructed PdCu (111) surface models with varying degrees of tensile strain for DFT calculations.

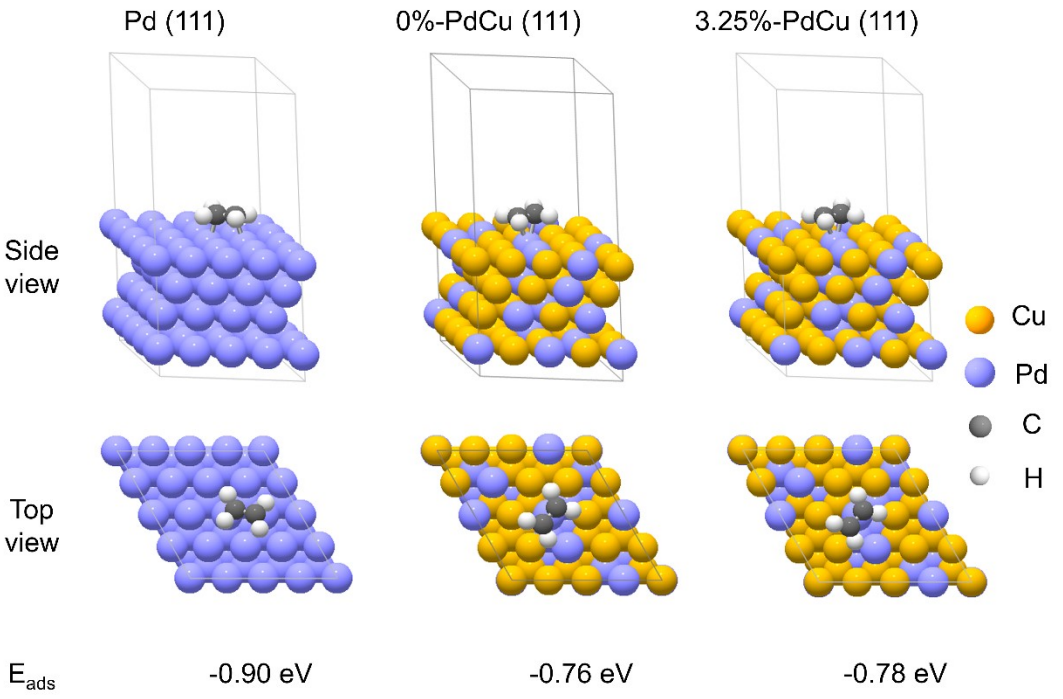

Figure S23. Adsorption energies (E_{ads}/eV) of C_2H_4 on the Pd (111) surface, the 0%-PdCu (111) surface, and the 3.25%-PdCu (111) surface.

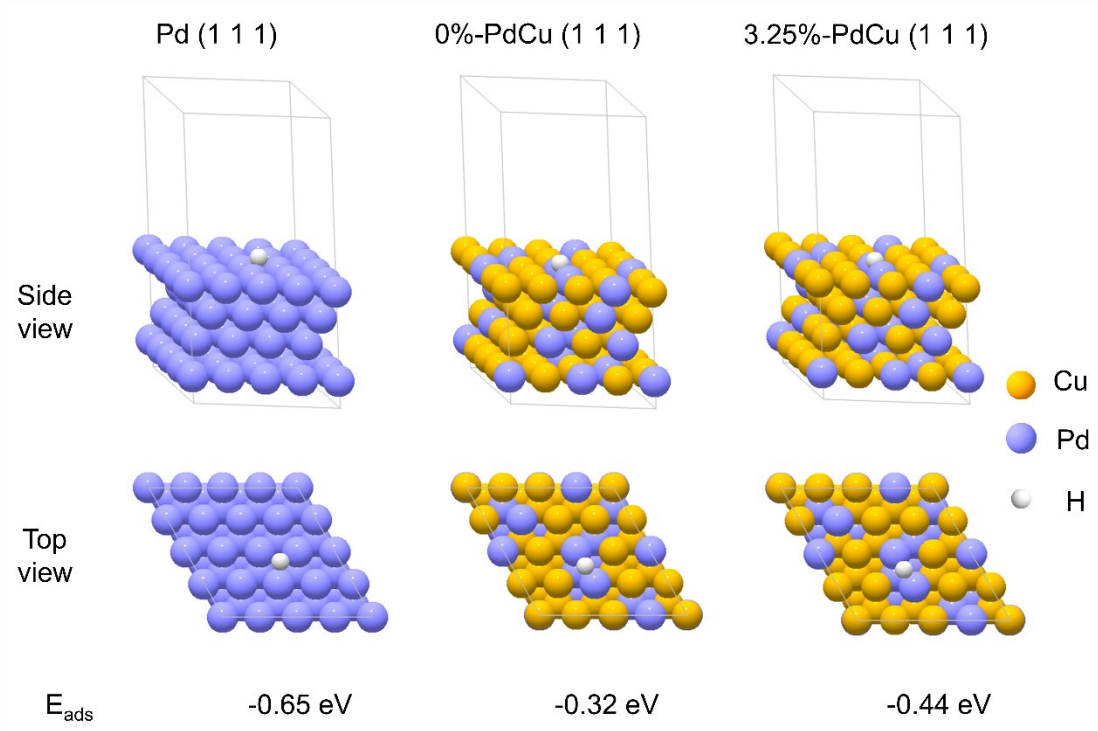

Figure S24. Adsorption energies (E_{ads}/eV) of hydrogen on the Pd (1 1 1) surface, the 0%-PdCu (1 1 1) surface, and the 3.25%-PdCu (1 1 1) surface.

4 References

(1) Ravel, B.; Newville, M. ATHENA, ARTEMIS, HEPHAESTUS: data analysis for X-ray absorption spectroscopy using IFEFFIT. *Journal of Synchrotron Radiation* **2005**, 12, 537-541.

(2) Qiu, X.; Thompson, J. W.; Billinge, S. J. L. PDFgetX2: a GUI-driven program to obtain the pair distribution function from X-ray powder diffraction data. *J. Appl. Crystallogr.* **2004**, 37, 678.

(3) Farrow, C. L.; Juhas, P.; Liu, J. W.; Bryndin, D.; Božin, E. S.; Bloch, J.; Proffen, T.; Billinge, S. J. L. PDFfit2 and PDFgui: computer programs for studying nanostructure in crystals. *J. Phys.: Condens. Matter* **2007**, 19, 335219.

(4) Tucker, M.; Dove, M.; Goodwin, A.; Keen, D.; Playford, H.; Slawinski, W. A. RMCProfile User Manual. *Code version* **2014**, 6, 0-155.

(5) Proffen, T.; Neder, R. B. DISCUS: a program for diffuse scattering and defect-structure simulation. *J. Appl. Crystallogr.* **1997**, 30, 171-175.

(6) Kresse, G.; Furthmüller, J. Efficiency of ab-initio total energy calculations for metals and semiconductors using a plane-wave basis set. *Comput. Mater. Sci.***1996**, 6, 15−50.

(7) Kresse, G.; Furthmüller, J. Efficient iterative schemes for ab initio total-energy calculations using a plane-wave basis set. *Phys. Rev. B* **1996**, 54, 11169.

(8) Blöchl, P. E. Projector augmented-wave method. *Phys. Rev. B* **1994**, 50, 17953.

(9) Perdew, J. P.; Burke, K.; Ernzerhof, M. Generalized gradient approximation made simple. *Phys. Rev. Lett.* **1996**, 77, 3865.

(10) Delley, B. J. An all-electron numerical method for solving the local density functional for polyatomic molecules. *Chem. Phys.* **1990**, 92, 508–517.

(11) Li, R.; Yue, Y.; Chen, Z.; Chen, X.; Wang, S.; Jiang, Z.; Wang, B.; Xu, Q.; Han, D.; Zhao, J. Selective hydrogenation of acetylene over Pd-Sn catalyst: Identification of Pd_2Sn intermetallic alloy and crystal plane-dependent performance. *Appl. Catal., B* **2020**, *279*, 119348.

(12) Ru, W.; Liu, Y.; Fu, B.; Fu, F.; Feng, J.; Li, D. Control of Local Electronic Structure of Pd Single Atom Catalyst by Adsorbate Induction. *Small* **2022**, 18, e2103852.

(13) Huang, F.; Deng, Y.; Chen, Y.; Cai, X.; Peng, M.; Jia, Z.; Ren, P.; Xiao, D.; Wen, X.; Wang, N.; et al. Atomically Dispersed Pd on Nanodiamond/Graphene Hybrid for Selective Hydrogenation of Acetylene. *J. Am. Chem. Soc.* **2018**, *140*, 13142-13146.

(14) Lee, S.; Shin, S.-J.; Baek, H.; Choi, Y.; Hyun, K.; Seo, M.; Kim, K.; Koh, D.-Y.; Kim, H.; Choi, M. Dynamic metal-polymer interaction for the design of chemoselective and long-lived hydrogenation catalysts. *Science Advances* **2020**, 6, eabb7369.

(15) Niu, Y.; Huang, X.; Wang, Y.; Xu, M.; Chen, J.; Xu, S.; Willinger, M. G.; Zhang, W.; Wei, M.; Zhang, B. Manipulating interstitial carbon atoms in the nickel octahedral site for highly efficient hydrogenation of alkyne. *Nat. Commun.* **2020**, *11*, 3324.

(16) Ma, J.; Xing, F.; Nakaya, Y.; Shimizu, K. I.; Furukawa, S. Nickel-Based High-Entropy Intermetallic as a Highly Active and Selective Catalyst for Acetylene Semihydrogenation. *Angew. Chem. Int. Ed.* **2022**, e202200889.

(17) Wei, S.; Liu, X.; Wang, C.; Liu, X.; Zhang, Q.; Li, Z. Atomically Dispersed Pd-N_1C_3 Sites on a Nitrogen-Doped Carbon Nanosphere for Semi-hydrogenation of Acetylene. *ACS Nano* **2023**, 17, 14831-14839.

(18) Gao, Q.; Yan, Z.; Zhang, W.; Pillai, H. S.; Yao, B.; Zang, W.; Liu, Y.; Han, X.; Min, B.; Zhou, H.; et al. Atomic Layers of B2 CuPd on Cu Nanocubes as Catalysts for Selective Hydrogenation. *J. Am.*

Chem. Soc. **2023**, 145, 19961-19968.
(19) Armbruster, M.; Kovnir, K.; Friedrich, M.; Teschner, D.; Wowsnick, G.; Hahne, M.; Gille, P.; Szentmiklosi, L.; Feuerbacher, M.; Heggen, M.; et al. $Al_{13}Fe_4$ as a low-cost alternative for palladium in heterogeneous hydrogenation. *Nat. Mater.* **2012**, *11*, 690-693.
(20) Zhang, L.; Ding, Y.; Wu, K. H.; Niu, Y.; Luo, J.; Yang, X.; Zhang, B.; Su, D. Pd@C core-shell nanoparticles on carbon nanotubes as highly stable and selective catalysts for hydrogenation of acetylene to ethylene. *Nanoscale* **2017**, *9*, 14317-14321.
(21) Huang, F.; Peng, M.; Chen, Y.; Cai, X.; Qin, X.; Wang, N.; Xiao, D.; Jin, L.; Wang, G.; Wen, X. D.; et al. Low-Temperature Acetylene Semi-Hydrogenation over the Pd_1-Cu_1 Dual-Atom Catalyst. *J. Am. Chem. Soc.* **2022**, 144, 18485-18493.
(22) Gao, R.; Xu, J.; Wang, J.; Lim, J.; Peng, C.; Pan, L.; Zhang, X.; Yang, H.; Zou, J. J. Pd/Fe_2O_3 with Electronic Coupling Single-Site Pd-Fe Pair Sites for Low-Temperature Semihydrogenation of Alkynes. *J. Am. Chem. Soc.* **2022**, *144*, 573-581.
(23) Ge, X.; Dou, M.; Cao, Y.; Liu, X.; Yuwen, Q.; Zhang, J.; Qian, G.; Gong, X.; Zhou, X.; Chen, L.; et al. Mechanism driven design of trimer Ni_1Sb_2 site delivering superior hydrogenation selectivity to ethylene. *Nat. Commun.* **2022**, *13*, 5534.
(24) Shao, L.; Zhang, W.; Armbruster, M.; Teschner, D.; Girgsdies, F.; Zhang, B.; Timpe, O.; Friedrich, M.; Schlogl, R.; Su, D. S. Nanosizing intermetallic compounds onto carbon nanotubes: active and selective hydrogenation catalysts. *Angew. Chem. Int. Ed.* **2011**, *50*, 10231-10235.
(25) Gu, J.; Jian, M.; Huang, L.; Sun, Z.; Li, A.; Pan, Y.; Yang, J.; Wen, W.; Zhou, W.; Lin, Y.; et al. Synergizing metal-support interactions and spatial confinement boosts dynamics of atomic nickel for hydrogenations. *Nat. Nanotechnol.* **2021**, 16, 1141-1149.
(26) Hu, M.; Zhao, S.; Liu, S.; Chen, C.; Chen, W.; Zhu, W.; Liang, C.; Cheong, W. C.; Wang, Y.; Yu, Y.; et al. MOF-Confined Sub-2 nm Atomically Ordered Intermetallic PdZn Nanoparticles as High-Performance Catalysts for Selective Hydrogenation of Acetylene. *Adv. Mater.* **2018**, e1801878.
(27) Bridier, B.; Pérez-Ramírez, J. Cooperative Effects in Ternary Cu−Ni−Fe Catalysts Lead to Enhanced Alkene Selectivity in Alkyne Hydrogenation. *J. Am. Chem. Soc.* **2010**, *132*, 4321-4327.
(28) Pei, G. X.; Liu, X. Y.; Wang, A.; Lee, A. F.; Isaacs, M. A.; Li, L.; Pan, X.; Yang, X.; Wang, X.; Tai, Z.; et al. Ag Alloyed Pd Single-Atom Catalysts for Efficient Selective Hydrogenation of Acetylene to Ethylene in Excess Ethylene. *ACS Catalysis* **2015**, *5*, 3717-3725.
(29) Feng, Q.; Zhao, S.; Xu, Q.; Chen, W.; Tian, S.; Wang, Y.; Yan, W.; Luo, J.; Wang, D.; Li, Y. Mesoporous Nitrogen-Doped Carbon-Nanosphere-Supported Isolated Single-Atom Pd Catalyst for Highly Efficient Semihydrogenation of Acetylene. *Adv. Mater.* **2019**, 31, e1901024.
(30) He, Y.; Liu, Y.; Yang, P.; Du, Y.; Feng, J.; Cao, X.; Yang, J.; Li, D. Fabrication of a PdAg mesocrystal catalyst for the partial hydrogenation of acetylene. *J. Catal.* **2015**, 330, 61-70.